Nano Energy 129 (2024) 110043

Contents lists available at ScienceDirect

Nano Energy

journal homepage: www.elsevier.com/locate/nanoen

Tribovoltaic nanogenerators based on n-n and p-p semiconductor homojunctions☆

Xiongxin Luo [a,b,1], Haixin Li [a,b,1], Andy Berbille [a,b], Lindong Liu [a], Yikui Gao [a,b], Gaosi Han [a,b], Zhong Lin Wang [a,b,c,*], Laipan Zhu [a,b,*]

[a] Beijing Key Laboratory of Micro-nano Energy and Sensor, Center for High-Entropy Energy and Systems, Beijing Institute of Nanoenergy and Nanosystems, Chinese Academy of Sciences, Beijing 101400, PR China

[b] School of Nanoscience and Engineering, University of Chinese Academy of Sciences, Beijing 100049, PR China

[c] School of Material Science and Engineering, Georgia Institute of Technology, Atlanta, GA 30332, United States

ARTICLE INFO

Keywords:
Tribovoltaic nanogenerator
Homojunction
Interface optimization
Laser-cutting
Surface state

ABSTRACT

Tribovoltaic nanogenerators (TVNGs) usually consist of two heterogeneous materials with disparate Fermi levels. However, TVNGs based on two same semiconductors with uniformed Fermi levels have been rarely reported, as they are believed to lack the sufficient potential difference necessary to drive tribo-induced carriers' separation and collection, resulting in minimal or negligible electricity production. Here, tribovoltaic nanogenerators based on two homojunction semiconductors (H-TVNGs) with the same doping concentration are proposed and designed. The H-TVNGs were demonstrated to be driven by abundant surface states introduced through laser cutting at the slider boundaries and surfaces, which further lead to the bending of interface energy bands. Upon two sliders of different sizes (with different degrees of band bending) come into contact, the built-in electric field at the interface will be established and drive tribo-induced carriers, leading to the production of a direct-current (DC) electrical signal. The performance of H-TVNGs could be effectively amplified or regulated by many factors, including laser cutting power, semiconductor surface roughness, slider shape, and the interface media, etc. These compelling findings reveal innovative physics in tribovoltaic effect, offer special insights for designing high-performance TVNGs, and provide effective strategies for device output optimization.

1. Introduction

The used of traditional fossil fuels present issues such as environmental degradation and resource depletion, urging the human developing the green and renewable energy sources to gradually supplant fuel consumption and achieve the "carbon peaking and carbon neutrality goals" [1,2]. While traditional renewable energy sources such as solar and wind energy are infinitely influenced by environmental factors and required batteries for energy storage, resulting in limited operational flexibility and low energy utilization efficiency [3,4]. The triboelectric nanogenerators (TENGs) have revolutionized energy harvesting by converting movement energy into electrical energy through triboelectricity and electrostatic induction principles. This innovative technology offers unparalleled advantages, including flexibility, portability, zero emissions, environmental sustainability, and efficiency [5,6]. However, there is a challenge that its composition of polymer materials with inherent high internal resistance impedance mismatches with commonly used electrical appliances [7,8]. The tribovoltaic nanogenerators (TVNGs) are typically constructed from an N-type and a P-type semiconductor materials, whose device properties closely match the impedance characteristics of household electrical devices [9–11].

In 2018, Liu et al. observed the generation of a direct current (DC) power in dynamic metal/MoS_2 heterojunctions [12]. Subsequently, in 2019, Wang et al. elucidated this phenomenon and coined it the

☆ Prof Zhong Lin Wang, an author on this paper, is the Editor-in-Chief of Nano Energy, but he had no involvement in the peer review process used to assess this work submitted to Nano Energy. This paper was assessed, and the corresponding peer review managed by Professor Chenguo Hu, also an Associate Editor in Nano Energy.

* Corresponding authors at: Beijing Key Laboratory of Micro-nano Energy and Sensor, Center for High-Entropy Energy and Systems, Beijing Institute of Nanoenergy and Nanosystems, Chinese Academy of Sciences, Beijing 101400, PR China.

E-mail addresses: zlwang@gatech.edu (Z.L. Wang), zhulaipan@binn.cas.cn (L. Zhu).

[1] These authors contributed equally.

https://doi.org/10.1016/j.nanoen.2024.110043
Received 4 June 2024; Received in revised form 4 July 2024; Accepted 22 July 2024
Available online 23 July 2024

"tribovoltaic effect" [13]. This effect involves the release of bindingtons (quantum units of energy when two atoms contact and then form a complete bond) during the friction between two semiconductor materials, thereby exciting electron-hole pairs at the sliding interface. The built-in electric field then facilitates the separation and expulsion of these pairs from the junction, resulting in a continuous DC current. In recent years, researchers improved the output performance of TVNG and extended its service life by increasing contact efficiency, introducing light and magnetic fields, and lubricating the friction interface [14–20]. Moreover, the tribovoltaic effect has been observed at various interfaces, including metal-semiconductor, metal-insulator-semiconductor, semiconductor-semiconductor, liquid-solid, and flexible interfaces [21–25]. TVNGs based on two same semiconductors with uniformed Fermi levels have been rarely reported, as there is generally no significant electric potential difference to drive charge separation and collection, resulting in little or no electricity production. Lu et al. [26]

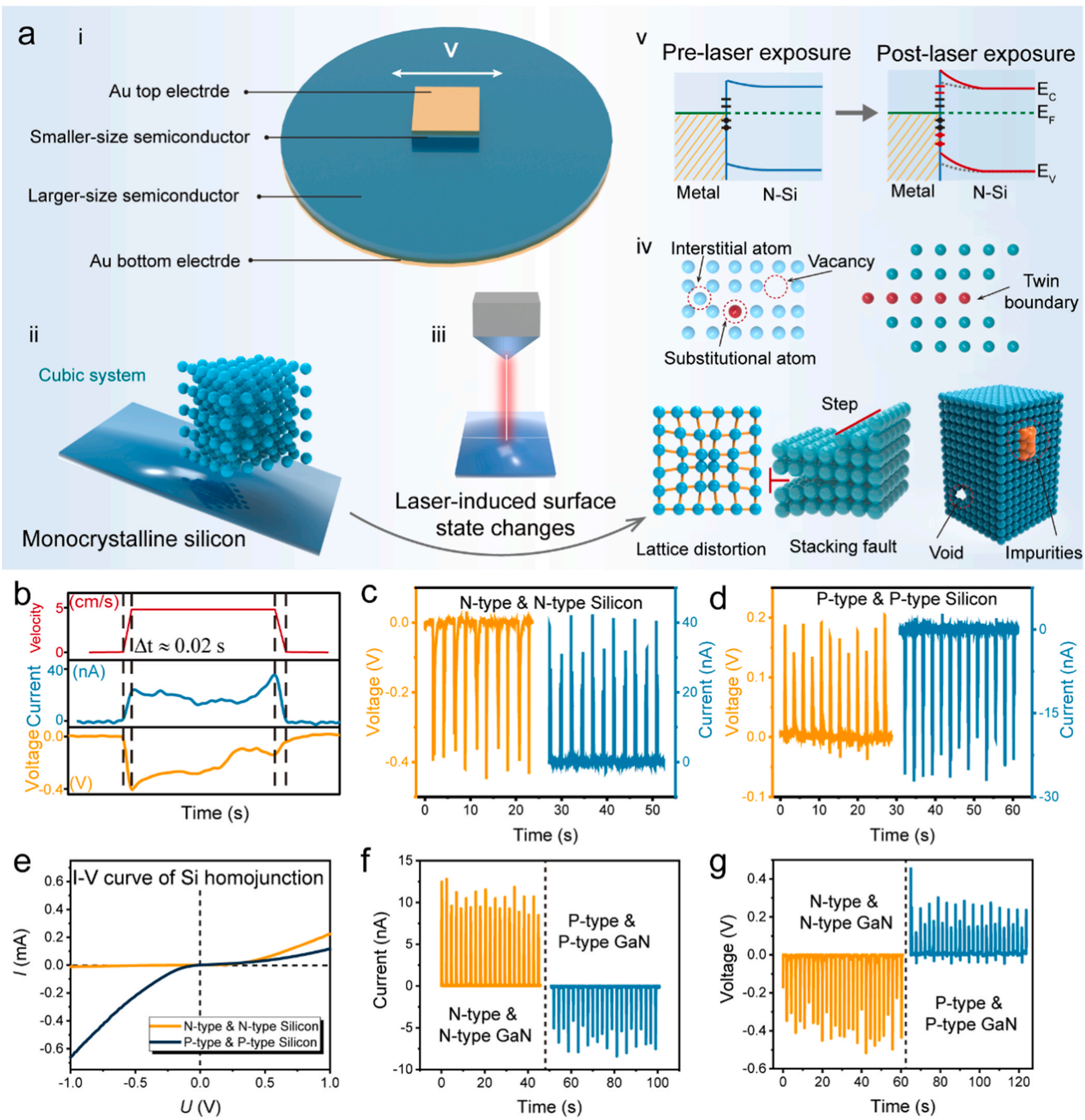

Fig. 1. Structure design and electric output characteristics of the H-TVNGs. (a) Design principles and basic structure of the H-TVNG: (i) three-dimensional (3D) schematic of the H-TVNG structure, (ii) schematic crystal structure of monocrystalline silicon, (iii) schematic diagram of laser-cutting induced surface state changes in silicon wafer, (iv) schematic diagram of laser-induced dislocations and defects in monocrystalline silicon, and (v) schematic diagram of band bending changes before and after laser cutting. (b) Basic DC characteristics of open-circuit voltage and short-circuit current of the H-TVNG. (c-d) Open-circuit voltage and short-circuit current as a function of time for N-type silicon H-TVNG (c) and P-type silicon H-TVNG (d). (e) I-V curves of N-type and P-type silicon H-TVNGs, respectively. (f-g) Short-circuit current (f) and open-circuit voltage (g) as a function of time for H-TVNGs based on GaN homojunctions.

reported a dynamic homojunction structure with the same semiconductor type and majority carrier type while different doping densities, and found that the dynamic NN homojunction with different Fermi levels exhibited higher carrier mobility than the PN or PP homojunction. However, this homojunction also entails complex semiconductor material doping and preparation processes. It will be much desired if a TVNG can be achieved based on two semiconductors with the same doping type as well as density, which will effectively simplify the device fabrication processes.

Here, we use two pieces of the same silicon wafer but with different sizes to create a homojunction TVNG, named H-TVNG. Surprisingly, a large output can even be realized in this H-TVNG due to the design and introduction of surface states between the larger and smaller silicon wafers. Upon contact, surface states at the smaller wafer boundaries induce a built-in electric field that drives triboelectric carriers, leading to the production of a DC signal. Our exploration of experimental conditions disclosed several ways to enhance or regulate the output of H-TVNG. We first revealed that the N- and P-type H-TVNGs output opposite directions in current. Additionally, we found that different cutting methods, laser irradiation power densities, and friction coefficient impact greatly the H-TVNG output. Moreover, we demonstrated that the deformation degree affects the output of H-TVNG when using sliders of different lengths and widths but with the same area. Finally, by introducing various interface liquid media, an external triboelectric field can be introduced to adjust the overall interface electric field and hence tune the H-TVNG output.

2. Results and discussion

2.1. Design of direct current TVNGs based on semiconductor homojunctions

Since their inception, the majority of TVNGs have typically featured heterogeneous structures [27]. When two dissimilar materials come into contact, a discrepancy in Fermi levels arises, propelling the free diffusion of carriers within the semiconductor materials, and then a built-in electric field is formed to make the heterojunction reach equilibrium. This built-in electric field serves as the driving force behind the migration of tribovoltaic charges [28]. In this study, an innovative homojunction H-TVNG was conceptualized. This design comprises two pieces of semiconductors with different sizes yet sharing the same semiconductor wafer (that is, sharing the same doping type as well as density), alongside top and bottom Au electrodes (Fig. 1a(i)). The meticulous fabrication process of the two sliders for H-TVNG is illustrated in Fig. S1, Supporting Information. Initially, an infrared laser was employed to intricately carve out two silicon wafers of different sizes on a doped silicon wafer. Subsequently, metal Au was deposited onto the carved silicon wafer surface using a magnetron sputtering technology, serving as the top and bottom electrodes. Consequently, smaller and larger sliders were obtained for the H-TVNGs. The monocrystalline silicon chosen for experiment possesses a cubic crystal structure, as shown in Fig. 1a(ii). X-ray diffraction (XRD) and Raman spectra are presented in Fig. S2, Supporting Information. Laser cutting, as shown in Fig. 1a (iii), induces alterations in surface states density of the cutting boundaries of the monocrystalline silicon. These surface states primarily stem from the stress and thermal impacts introduced at the cutting edges, resulting in the distortion of the silicon lattice and the generation of crystal defects like vacancies, twin boundaries, stacking faults, impurities, etc (Fig. 1a(iv)) [29–32]. Scanning electron microscopy (SEM) image of the silicon wafer surface post-exposure to the laser is presented in Fig. S3, Supporting Information, revealing the emergence of minute cracks and protrusions [30]. These lattice distortions and defects form unsaturated bonds and localized electronic states, ultimately influencing the electronic structure and electron transport properties of semiconductors. Schematic energy band structures for pre- and post-laser exposure are plotted in Fig. 1a(v). Following laser irradiation, the crystal surface exhibits an enhancement of surface states, prompting an upward curvature in the energy band and the formation of a stronger built-in electric field.

Electrical signals generated from a typical H-TVNG are shown in Fig. 1b. Similar to other heterojunction TVNGs, it maintains DC characteristics in output voltage and current at a fixed sliding speed. We conducted experiments using two widely used semiconductor materials, Si and GaN, to construct H-TVNGs and analyzed the outputs. The results of the Si-based H-TVNGs are depicted in Figs. 1c and 1d. Following laser-induced surface states modulation of silicon wafers, the N-type silicon-based H-TVNG with upper slider's area of $2 \times 2\ \mathrm{cm}^2$ yields electrical signals of -0.4 V and $+40$ nA. Conversely, the P-type silicon-based H-TVNG produces electrical signals of $+0.2$ V and -25 nA, showing a reversed output direction to the case of N-type. A comparison between the two silicon-based H-TVNGs reveals a slightly superior output in the N-type variant, attributed to the higher carrier mobility for the N-type semiconductors [26]. To understand this phenomenon, we measured the I-V curves of these two H-TVNGs, as shown in Fig. 1e. It is observed that the N-type homojunction demonstrates positive rectification characteristics, whereas the P-type homojunction exhibits negative. This observation is derived from the distinct energy band structures of two silicon wafers with post-laser exposure. Their interaction leads to the formation of junctions, forming built-in electric fields that propel the directional migration of electron-hole pairs. Furthermore, similar output patterns to those observed with silicon wafers were discovered in H-TVNGs based on gallium nitride (GaN) epitaxial films on sapphire wafers, as shown in Figs. 1f and 1g, demonstrating that it is a common phenomenon for various monocrystal semiconductors.

2.2. Electric output characteristics of the H-TVNGs

To further investigate the electrical output characteristics of H-TVNGs. Initially, we examined the influence of various vertical pressures and slider sliding speeds on the output of TVNG, as depicted in Fig. S4, Supporting Information. It is evident that both the output current and voltage of the H-TVNG increase with higher speeds and pressures. However, excessive speed and pressure will lead to excessive wear. Therefore, for all subsequent experiments, a vertical stress of 5 N and a speed of 10 cm/s were selected. Then, we conducted comparative experiments using several sliders of various sizes. First, in the case of N-type H-TVNG (as shown in Fig. 2a, b), it is obvious that the currents are uniformly positive while the voltages are negative. As the upper slider area increases, the trend of the output current decreases. This phenomenon stems from the fact that, under the same vertical stress (5 N), the smaller slider undergoes greater pressure intensity at the interface. As a result, the boundaries of the smaller slider have more opportunities to interact with the larger one, potentially inducing additional surface states and thereby enhancing the output. Furthermore, I-V curves as shown in Fig. 2c confirm that smaller-area heterojunctions do indeed exhibit larger built-in electric fields. Additionally, for P-type H-TVNG (shown in Fig. 2d-f), the directions of current and voltage exhibit opposite to that of the N-type one. Similarly, as the area increases, the output decreases. We conducted measurements on H-TVNGs with stator areas of 40 cm^2, 60 cm^2, and 80 cm^2, all while maintaining a constant slider area of 4 cm^2. The experimental results, as shown in Fig. S5, Supporting Information, demonstrated that the output of the H-TVNGs remained essentially unchanged despite the variations in stator area. This can be attributed to the laser cutting process of the silicon wafer, which induces lattice defects or distortions only in a localized area near the laser beam, thereby generating abundant surface states. Moreover, the small slider consistently remains centered within the larger stator and does not slide towards its edges, ensuring stable output across different stator sizes. Consequently, these H-TVNGs exhibit consistent performance irrespective of the stator area.

We can then propose the working mechanism of the H-TVNGs. In the case of N-type H-TVNG, the external current always flows from the

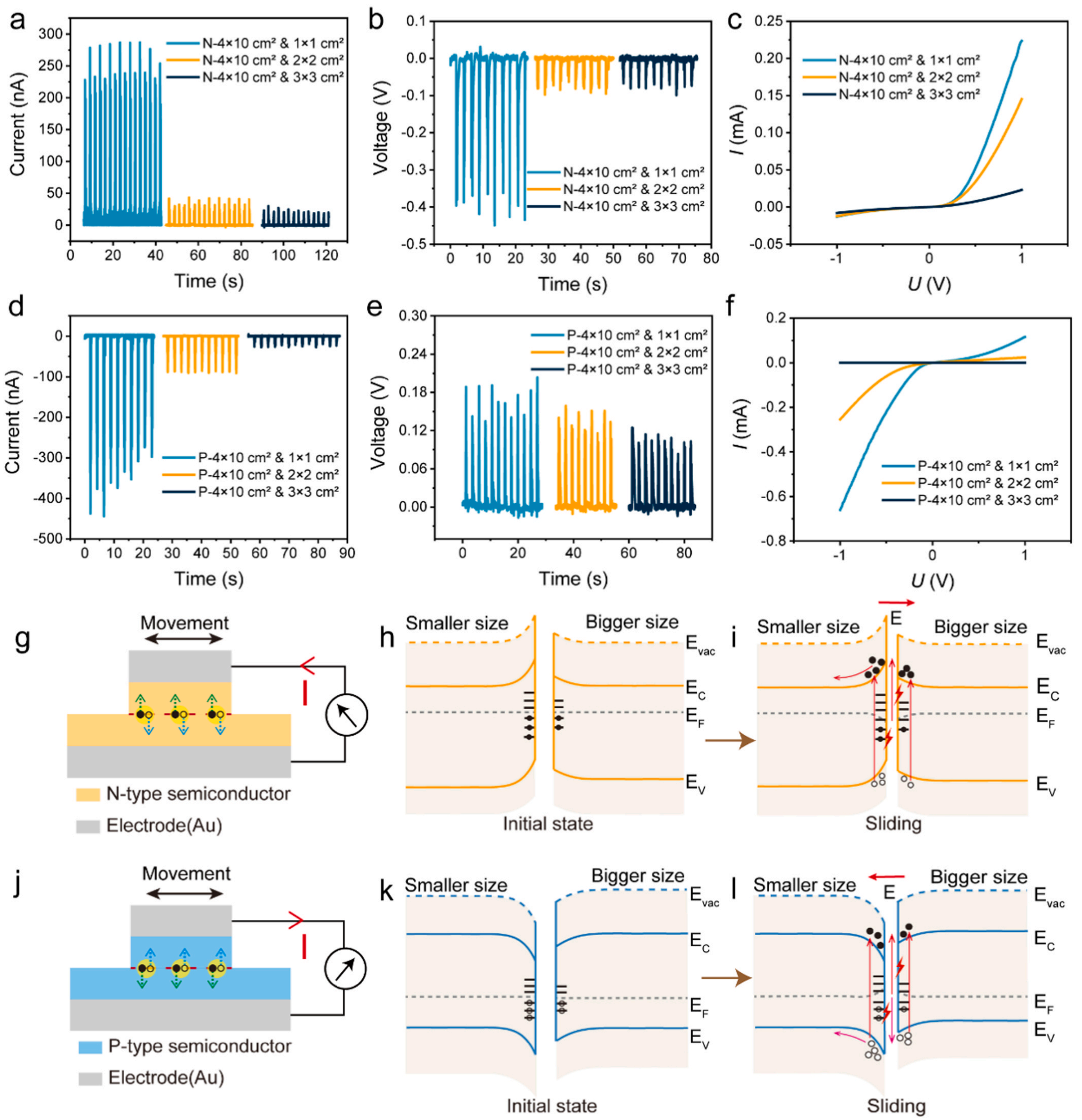

Fig. 2. Electric Output Characteristics and the proposed mechanism of the H-TVNG. (a-b) Output short-circuit current (a) and open-circuit voltage (b) of the N-type H-TVNG with different slider sizes under a vertical force of 5 N. (c) I-V characteristics of the N-type homojunction with different sizes. (d-e) Output short-circuit current (d) and open-circuit voltage (e) of P-type H-TVNG with different slider sizes under a vertical force of 5 N. (f) I-V characteristics of the P-type homojunction with different sizes. (g) Schematic carriers drifting and current flowing of an N-type H-TVNG. (h, i) Schematic mechanism denoting carrier generation and transfer between the smaller and bigger size N-type silicon wafers under static (h) and dynamic states (i), respectively. (j) Schematic carriers drifting and current flowing of a P-type H-TVNG. (k, l) Schematic mechanism denoting carrier generation and transfer between the smaller and bigger size P-type silicon wafers under static (k) and dynamic states (l), respectively.

larger-sized semiconductor to the smaller-sized semiconductor (slider), as shown in Fig. 2g. It is attributed to the rich surface states induced during the laser-cutting of the wafer boundaries. At the contact location, the smaller semiconductor undergone a greater temperature change under the same laser power and possesses a higher surface state density compared to that of the bigger size (Fig. S6, Supporting Information), which leads to a greater energy band curvature, while the larger size band curvature is smaller (Fig. 2h). When the two silicon wafers are in close contact, electrons diffuse in the depletion layer, forming a built-in electric field directed from the large-sized semiconductor to the small-sized semiconductor. And then, the kinetic energy of the sliding breaks the bonds at the interface due to the tribovoltaic effect when two silicon wafers slide against each other. Subsequently, the newly formed bonds release a lot of bindingtons, which are absorbed by a large number of electrons trapped in the surface states. The electrons that have absorbed the bindingtons are excited to the conduction band and then transferred from the larger semiconductor to the smaller semiconductor driven by the built-in electric field, thereby generating a directional current (Fig. 2i). Conversely, the external current direction of the P-type H-TVNG is opposite with that of the N-type case, always flowing from the smaller-sized semiconductor to the larger-sized semiconductor (Fig. 2j). For P-type H-TVNG, there are more abundant surface states on smaller semiconductor, resulting in holes being generated at the interface and driven away inside the bulk of the smaller semiconductor, while electrons are trapped into the interface. The direction of the built-in electric field generated is exactly opposite to that of the N-type case, thus leading to the generation of electrical output in the opposite direction (Fig. 2k, l).

2.3. Verification of laser-cutting-induced changes in surface state density

To verify that laser-cutting can induce changes in the surface state density of semiconductor, we conducted the following verification experiments. Firstly, diamond knife and laser were employed to cut silicon wafers with identical sizes, respectively. The comparison test results are shown in Fig. 3a and b. Experimental findings reveal that the short-circuit current and open-circuit voltage of the H-TVNG composed of knife-cut silicon wafers were merely 9 nA and 15 mV, respectively. In contrast, H-TVNG composed of laser-cut silicon wafers exhibited significantly higher output short-circuit current and open-circuit voltage, reaching up to 35 nA and 50 mV, respectively, which indicates a four-fold increase compared to that of the knife-cut one. I-V curves of the homojunction composed of silicon wafers cut using the two different methods also demonstrate that the homojunction composed of laser-cut silicon wafers possesses a higher Schottky barrier and hence can generate a larger built-in electric field (as shown in Fig. 3c). To verify the feasibility of extending surface state control to other heterojunction TVNGs, we conducted experiments using two sliders with different cutting methods. Remarkably, we achieved a similar improvement in output as observed in homojunction TVNGs, as shown

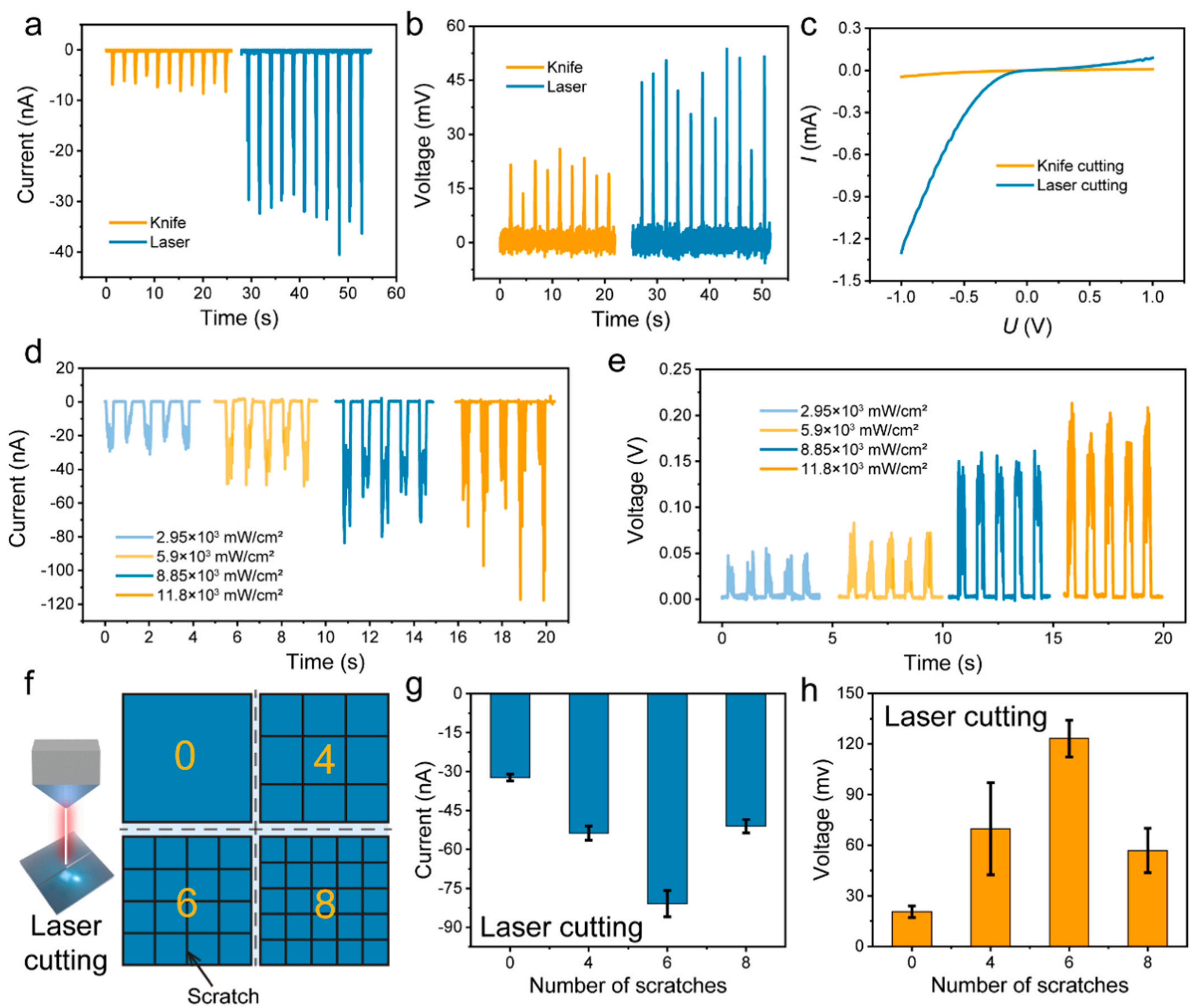

Fig. 3. Comparison of the output performance of the H-TVNGs composed of semiconductors processed by different cutting methods. (a-b) Short-circuit current (a) and open-circuit voltage (b) of the H-TVNGs with different cutting methods. (c) I-V characteristics of the H-TVNGs with different cutting methods. (d-e) Short-circuit current (d) and open-circuit voltage (e) of the H-TVNGs composed of silicon wafer sliders cut at various laser power densities. (f) Schematic of laser exposure leaving different numbers of scratches on the surface of silicon wafers. (g-h) Short-circuit current (g) and open-circuit voltage (h) of the H-TVNGs with scratch numbers of the upper sliders of 0, 2, 4, 6, and 8, respectively.

in Fig. S7, Supporting Information. Furthermore, we also examined the output of H-TVNGs composed of silicon wafers cut at various laser power densities and cutting times, as shown in Fig. 3d-e and Fig. S8 Supporting Information. It is evident that as the laser power density or laser cutting times increases, both the short-circuit current and open-circuit voltage of the H-TVNG exhibit increasing trends. It can be attributed to the fact that a higher laser power or longer cutting times results in more defects at the cutting edges of the silicon wafers, consequently introducing larger surface state densities. The H-TVNG composed of such silicon wafers exhibits a stronger Schottky barrier, generating a larger built-in electric field and then facilitating the separation and transportation of tribo-induced carriers.

Additionally, the surface states of the silicon wafers can also be controlled by varying laser exposed area. In this experiment, the silicon

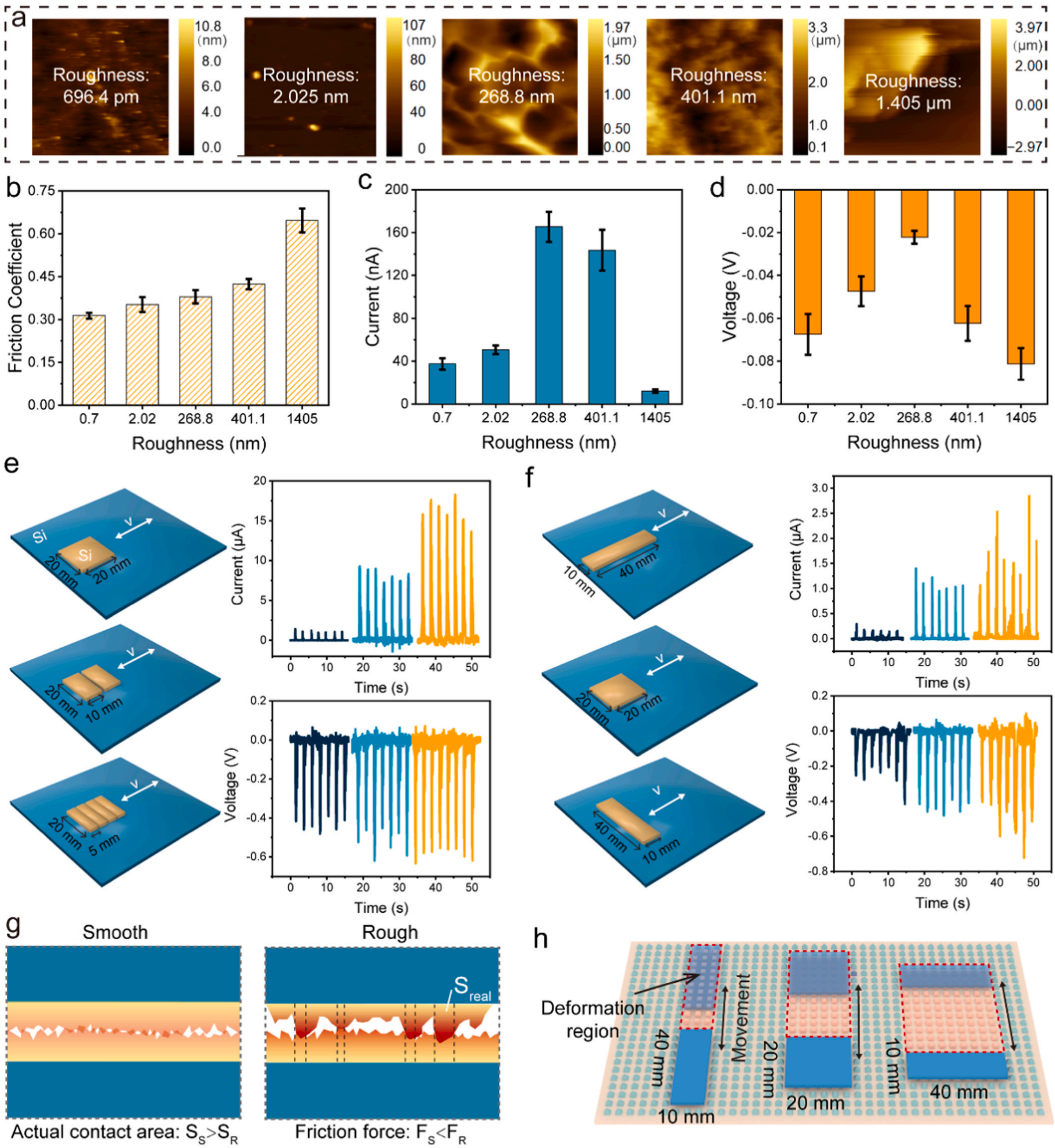

Fig. 4. Impacts of slider roughness and shape on the output performance of H-TVNGs. (a) AFM images of five types of silicon wafers with different roughness. (b) Friction coefficients of the above five silicon wafers. (c-d) Short-circuit current (c) and open-circuit voltage (d) of the H-TVNGs with varying roughness. (e) Output performance of H-TVNGs setting up by sliders with different parts but keeping the same overall contact area. (f) Output performance of H-TVNGs setting up by sliders with different ratios of length to width but keeping the same overall contact area. (g) Schematic diagram of the friction forces and effective contact areas for smooth and rough interfaces. (h) Illustrations of the generated deformation area for sliders with different ratios of length/width but keeping the same overall contact area.

wafers with the same size of 2×2 cm^2 were exposed by a laser radiation with 1064 nm wavelength and a constant power density of 8.85 mW/cm^2. High-power laser exposure will leave different numbers of scratches on the surface of the silicon wafer slider, which can reflect the exposure area based on the number of scratches. Sliders with scratch numbers of 0, 2, 4, 6, and 8, were fabricated, respectively, as shown in Fig. 3f. The output results are depicted in Figs. 3g and 3h. It is apparent that as the exposed area increases, the output of H-TVNG initially shows an increasing trend first, and then reaching a maximum when the number of scratches is 6, which is due to that larger laser exposure areas induce more surface states. However, as the exposed area further increases, both the short-circuit current and open-circuit voltage begin to decline. It is speculated that this may be due to laser exposure causing deeper depressions on the silicon wafer's surface, which affects the contact efficiency of surface states of the two rubbing semiconductors. Inspired by this, in subsequent experiments, the influence of semiconductor surface roughness (friction coefficient) on the output of H-TVNG was examined.

2.4. Impacts of slider roughness and shape on the output performance of H-TVNGs

Five P-type silicon wafers with the same doping density (resistance of 0.1–0.5 Ω·cm) but different roughness were utilized to investigate the correlation between the slider's friction coefficient and the output performance. Firstly, the surface morphologies of these silicon wafers were characterized using atomic force microscopy (AFM) images, as shown in Fig. 4a. The roughness measurements yielded a value of 696.4 pm, 2.025 nm, 268.8 nm, 401.1 nm, and 1.405 μm for the as-used silicon wafers. Subsequently, the wafers with different roughness were rubbed against a standard silicon wafer without special treatment to obtain the friction coefficient, and the results are presented in Fig. 4b. It can be seen that as the roughness of the slider increases, the friction coefficient also reveals an increasing trend. Following this, these five silicon wafers were employed as sliders to fabricate corresponding H-TVNGs, whose output results were illustrated in Figs. 4c and 4d. A notable observation is that as the roughness increases, the short-circuit current initially shows an increasing trend followed by a decrease, consistent with the earlier findings on different scratches. However, the open-circuit voltage exhibits an opposite trend to that of the short-circuit current, decreasing first and then increasing. Furthermore, under the condition of maintaining a constant total contact area, the slider was segmented into different parts, which were connected in series to form an upper slider of the H-TVNG for output testing, as shown in Fig. 4e. It was noted that as the slider was divided into more segments, the output current progressively increased, with the voltage also displaying an increasing trend. Additionally, the outputs of H-TVNGs with sliders of various ratios of length to width but keeping a constant area (40 mm^2) were examined, as shown in Fig. 4f, where it can be concluded that the H-TVNG with a longer length perpendicular to the sliding direction results in a larger output.

Further investigation was conducted to comprehend these phenomena. First, for demonstrating the phenomenon of the change of the output electrical signal of H-TVNG with the roughness of the slider, I-V characteristics using these siders with different roughness were tested, as shown in Fig. S9, Supporting Information. As the roughness of the slider increases, the Schottky barrier of the junction first decreases and then increases, mirroring the trend observed in the open-circuit voltage signal obtained experimentally (Fig. 4d). We guess that as surface roughness escalates, the density of interface states concurrently increases, thereby strengthening the built-in electric field. However, when the slider is relatively smooth, the primary impact of the oxide layer on the surface of the silicon wafer might further enhance the density of interface states, thus reinforcing the built-in electric field. Hence, the built-in electric field strength reflects the output open-circuit voltage of H-TVNG. Short-circuit current mainly depends on carrier transport, which is closely related to the conductive properties of the material. We established the following relationship between output current and friction coefficient of the H-TVNG:

$I \propto F_f \, S_{real}$,

where I is the short-circuit current of the H-TVNG, S_{real} represents the actual contact area between the two sliders, and F_f denotes the friction force. The friction force is positively correlated with the friction coefficient. On the one hand, the frictional force displays a positive correlation with the output current of TVNG. This is because when the upper slider moves under greater frictional force, the interface gains more energy, thereby stimulating the excitation and separation of more electron-hole pairs to form a DC current. However, on the other hand, due to the rougher surfaces of the sliders, the efficiency of interface contacts decreases, resulting in a reduction of the actual contact area, thus diminishing the output current. Therefore, with a smooth surface, the effective contact area of TVNG is larger, that is, $S_S>S_R$, but the friction force obtained is smaller, that is $F_S<F_R$ (left inset of Fig. 4g). Conversely, on a rough surface, the effective contact area of H-TVNG decreases, but the friction force is larger (right inset of Fig. 4g). Therefore, the output current of the H-TVNG with different slider roughness will reach an optimal value, as the experiments indicated. It is noteworthy that the electrical conductivity of silicon wafers is related to the crystal phase. The references show that the electrical conductivity of single crystal silicon in the <111> direction is superior to that in the <001> direction[33]. In our devices, we specifically chose silicon wafers grown along the <001> crystalline phase. Consequently, for rough silicon wafers, accessing the sides closer to the <111> crystal phase is facilitated, as illustrated in Fig. S10, Supporting Information. Therefore, using a rougher slider, the conductivity of the H-TVNG increases and the current output is larger.

In addition, with the same area of sliders, when the sliding direction is perpendicular to a longer side, the output will increase, which is attributed to the influence of the degree of deformation (Fig. 4h). Given the side length perpendicular to the sliding direction is a, when the slider slides in a distance of L, there will be a deformation on the material surface with a total deforming area of aL. Given a larger side length of b (where b>a, and the overall area of slider is unchanged), the generated deformation area at this situation is bL. Therefore, the sliding deformation is larger when the longer side length perpendicular to the sliding direction is applied. The greater deformation generates more bindingtons at the contacting interface, and then the released bindingtons excites many more carriers, resulting in a greater electrical output of H-TVNGs. These experimental results offer deep insights for designing high-performance TVNGs.

2.5. Modulating the output of H-TVNGs through liquid media

To further enhance the output of H-TVNGs, a liquid medium was introduced between the two sliders to optimize the contact interface. Initially, varying volumes of deionized water (DI water) were carefully injected at the interface of an N-type H-TVNG. It was found that the maximum output current was achieved with an interface liquid volume of 5 μL, as displayed in Fig. 5a. This particular volume proved to be optimal, as an excessive amount of liquid medium inevitably increases the contact resistivity, leading to a reduction in output current of the H-TVNG [18]. It shows an increase in short-circuit current by a factor of 4 compared with the case without deionized DI water medium (see Fig. S11, Supporting Information). Additionally, the introduction of pure ethanol at the interface led to some performance enhancement, although the effect was significantly lower than that observed with DI water (see Fig. 5b). Subsequently, a similar experiment was conducted using a P-type H-TVNG (see Fig. 5c). It revealed that adding DI water at the interface produced a short-circuit current opposite to that of no addition, while adding ethanol resulted in an enhanced current in the same direction. Therefore, to systematically investigate the impact of DI water and ethanol on the output of H-TVNGs at the interface, different

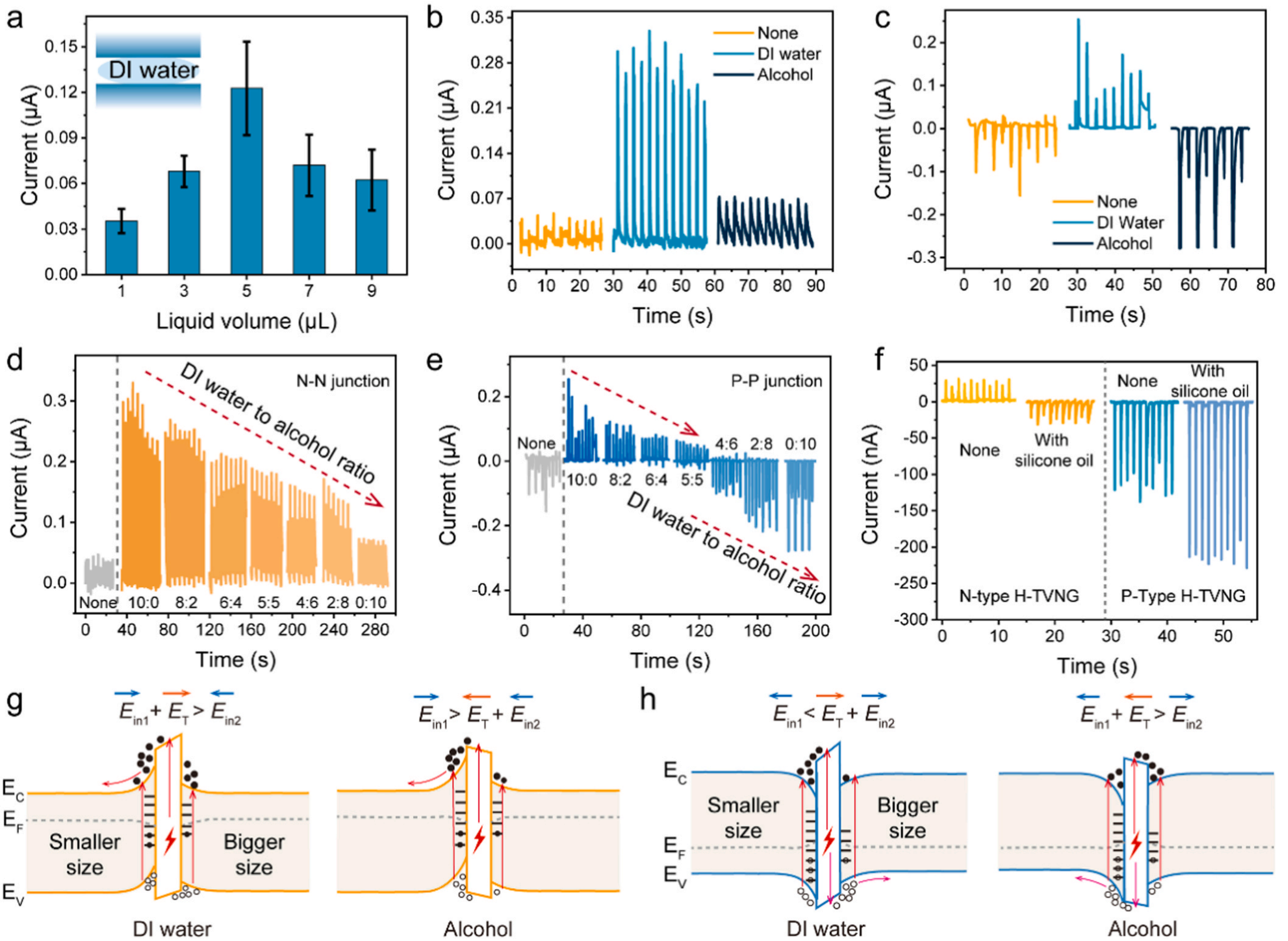

Fig. 5. Manipulation of output short-circuit current of the H-TVNGs by introduction of interface liquid media. (a) Short-circuit current of the H-TVNG intermediated with different DI water volumes. (c-d) Short-circuit current of the N-type (b) and P-type (c) H-TVNG with DI water and alcohol as interface media and without addition. (d-e) Short-circuit current of the H-TVNG composed of N-N homojunction (d) and P-P homojunction (e) with varying concentration ratio of DI water to alcohol. (f) Short-circuit current of H-TVNG with silicone oil as interface media. (g-h) Mechanisms of adding DI water and alcohol to the interface of N-type (g) and P-type (h) H-TVNGs to modulating the output performance.

proportions of ethanol and DI water were added to the two types of H-TVNGs, and the short-circuit current signals were recorded, as shown in Figs. 5d and 5e. For the N-type H-TVNG, it was observed that the addition of pure DI water (ratio 10:0) resulted in the highest output current. As the alcohol concentration increased, the output current gradually decreased and eventually returned to the original direction observed without any medium. For the P-type H-TVNG, the addition of pure DI water caused the current direction to reverse rapidly. As the alcohol concentration increased, the current gradually decreased, reached to a negative direction as the original state at a ratio of 4:6 (DI water to alcohol), and then gradually increased again towards the negative direction.

To further demonstrate the superiority of the interface liquid medium, the silicone oil, a commonly used lubricating oil, was introduced to the interface of H-TVNG following the previously outlined method. The short-circuit current was measured and shown in Fig. 5f. Similar to the effects observed with ethanol, the introduction of silicone oil resulted in not only an increase in the output current of H-TVNG but also the ability to modulating its output direction. Furthermore, silicone oil is a widely used lubricant, so it is foreseeable that its incorporation will likely not only enhance the output of TVNG but also contribute to the device's durability.

It is hypothesized that the modulation of the output of H-TVNGs is attributed to the involvement of an interface triboelectric field, as illustrated in Figs. 5g and 5h. Introducing liquid media introduces three electric fields that influence TVNG's output: the interface triboelectric field (E_T) resulting from the interaction between the droplet and the silicon wafer, along with two built-in electric fields. The build-in electric field arises from the interface contact between the smaller-sized silicon wafer and the droplet (E_{in1}), and between the larger-sized silicon wafer and the droplet (E_{in2}), respectively. Due to the higher surface state density of the smaller-sized silicon wafer in the contact area compared to the larger-sized silicon wafer, the equivalent (overall) direction of built-in electric field is in consistent with that of the small-sized side. Consequently, the subsequent discussion primarily pertains to the built-in electric field formed at the small-sized silicon wafer. For N-type H-TVNGs, the triboelectric field generated by the friction between DI water and N-type silicon aligns with the built-in electric field, thereby enhancing the output. In contrast, the friction between alcohol and N-type silicon generates a triboelectric field that opposes the built-in electric field. However, this triboelectric field is consistently smaller than the built-in electric field, resulting in a mere decrease in current output as the alcohol concentration increases, without a change in current direction. Furthermore, with the alcohol added, the internal resistance of the H-TVNG is expected to decrease, resulting in an output current exceeding that of the case without the droplet medium. In the case of P-type H-TVNGs, the friction between DI water and the silicon wafer produces a triboelectric field that is substantially larger than the built-in electric field and opposite in direction, leading to an increase in the reverse direction of the current. Conversely, the triboelectric field generated by the friction between alcohol and the P-type silicon wafer aligns with the built-in electric field, resulting in a larger current after adding alcohol compared to that without the liquid medium. It is not difficult to conclude that as the alcohol concentration increases, the triboelectric fields generated by water friction and alcohol friction, respectively, counteract each other, causing the output current to gradually decrease. Once the alcohol concentration reaches a certain level, the triboelectric field generated by alcohol friction dominates, causing the output current to reversely increase. To substantiate our conjecture, we designed an experiment depicted in Fig. S12, Supporting Information, where DI water and alcohol were applied on the silicon wafer for sliding charging, followed by detecting the deposition of the droplets after charging using the tip of a needle. The test results are presented in Fig. S13, Supporting Information. It is demonstrated that alcohol sliding on silicon wafer generates positive charges, whereas DI water sliding results in negative charges, consistent well with our hypothesis.

3. Conclusions

In summary, this study focuses on the design of TVNGs based on homojunctions with the same doping density, which exploits the difference in energy band bending resulting from laser-cutting induced lattice distortion and vast surface states in semiconductors. The electrical output characteristics of H-TVNGs are thoroughly investigated. For H-TVNGs composed of N-type silicon wafers, the external current consistently flows from the larger-sized wafer to the smaller-sized wafer, while the direction is reversed for the case of P-type silicon wafers. Additionally, the study examines the effects of various factors on the output of the H-TVNGs, including laser power, slider roughness, slider shape, and interface media, etc. Firstly, increasing laser-cutting power results in an enhanced output for H-TVNGs. Secondly, the roughness of the slider has a dual impact on H-TVNG. On the one hand, a rougher slider generates greater friction force, leading to increased accumulation of bindingtons at the interface and subsequently boosting the output. On the other hand, increased roughness reduces the effective contact area, resulting in a decrease in H-TVNG's output. Furthermore, the study identifies that sliding along the direction with the longer side perpendicular to the sliding direction leads to a higher output due to the larger deformation efficiency. Lastly, the introduction of interface liquid media, such as alcohol and DI water, allows for the manipulation of electrical output direction and magnitude of the H-TVNGs. These findings offer a range of convenient and effective methods to improve the output of TVNGs based on homojunctions, thus promoting their application potentials in self-powered sensing systems and high-entropy energy supply.

4. Experimental section

4.1. Materials

The silicon wafers with varying types and roughness levels were procured from Suzhou Jinggui Technology Co., Ltd., featuring specifications of 4 in. in size, crystal plane orientation along [001], a diameter of 100 ± 0.3 mm, a thickness of 500 ± 25 μm, and an electrical resistivity of 0.1–0.5 Ω·cm. The epitaxial GaN on sapphire substrate, purchased from Jingdian Semiconductor Material Co., Ltd. in China, boasts a size of 2 in., an epitaxial layer thickness of 4 μm, and a doping concentration of 5×10^{18} cm^{-3}. Analytically pure alcohol (99.7 %) was sourced from Shanghai Aladding Biochemical Technology Co., Ltd. DI water was prepared in the laboratory.

4.2. Fabrication of the H-TVNGs

To begin the fabrication process, the silicon wafers are shaped into specific forms using either a diamond dicing knife or the SFS20 laser dicing machine (with a wavelength of 1064 nm and a largest laser power density of 2.98×10^4 mW/cm^2), which was developed by Wuhan Sanggong Optoelectronic Equipment Manufacturing Company. Subsequently, the silicon wafers undergo a 5-minute immersion in 10 % hydrofluoric acid to eliminate the surface oxide layer. They are then thoroughly cleaned using alternating alcohol and DI water rinses. Next, a 50 nm-thick Au film layer is deposited onto the one side of the silicon wafer as the electrode. This is achieved through a magnetron sputtering process utilizing the Denton Discovery 635 system in an Ar gas environment for a duration of 10 min. The bottom and top electrodes are ultimately connected using Cu wires. For the GaN-based H-TVNGs, a similar procedure is followed, with the wafer being cut into desired shapes using the aforementioned methods. In this case, metal indium serves as the electrode and is directly connected to the Cu wire at the edge of the wafer.

4.3. Material characterization and electrical measurement of the H-TVNGs

For material characterizations, X-ray diffraction (XRD) patterns were acquired using an X-ray diffractometer (XPert3 Powder, Netherlands) operating at 40 kV, 40 mA, a step length of 0.02°, and a scanning speed of 0.5° s^{-1}. Raman spectra were captured employing a laser confocal Raman spectrometer (LabRAM HR Evolution) furnished with a × 50 objective lens, a 532 nm laser, and a grating of 1800 gr mm^{-1}. The surface morphology of the silicon wafer was scrutinized using a scanning electron microscope (Nova NanoSEM 450) with a 10 kV acceleration. The friction coefficient of various friction interfaces was assessed using a Bruker Universal Mechanical Tester (UMT TriboLab), maintaining an applied vertical pressure of 5 N and a sliding speed of 10 cm s^{-1}. For electrical measurement, a Keithley 4200 semiconductor test analyzer was utilized to measure the I-V characteristics of the homojunctions, scanning from −1–1 V with a sampling rate of 0.01. The electric signals of the H-TVNGs were measured using a Keithley 6514 electrometer. To facilitate sliding motion, a linear motor motion platform (Akribis Systems, SGL100-AUM3-S2-R10-CMNT Package) was employed, while a pressure tester (Handpi, HP-100) was utilized to gauge the vertical pressure test of the two sliding interfaces. In the absence of specific instructions, the upper slider's area was standardized at 2×2 cm^2, with a sliding speed of 10 cm s-1 and a vertical press of 5 N. All experiments were conducted under uniform lighting conditions in the same room, ensuring consistent light intensity throughout.

CRediT authorship contribution statement

Yikui Gao: Methodology, Investigation. **Gaosi Han:** Formal analysis, Data curation. **Andy Berbille:** Writing – review & editing, Methodology, Formal analysis. **Lindong Liu:** Methodology, Data curation. **Zhong Lin Wang:** Writing – review & editing, Supervision, Investigation, Funding acquisition. **Laipan Zhu:** Writing – review & editing, Supervision, Methodology, Investigation, Formal analysis. **Xiongxin Luo:** Writing – original draft, Methodology, Formal analysis, Data curation, Conceptualization. **Haixin Li:** Writing – original draft, Methodology, Formal analysis, Data curation.

Declaration of Competing Interest

The authors declare that they have no known competing financial interests or personal relationships that could have appeared to influence the work reported in this paper

Data availability

The authors do not have permission to share data.

Acknowledgements

This research was supported by the National Natural Science Foundation of China (Grants 52192610 and 52192613), National Key R & D Project from Minister of Science and Technology (2021YFA1201601).

Appendix A. Supporting information

Supplementary data associated with this article can be found in the online version at doi:10.1016/j.nanoen.2024.110043.

References

[1] P.R.a.M.R. Hannah Ritchie, Energy Production and Consumption, OurWorldInData.org (2020) ⟨https://ourworldindata.org/energy-production-consumption⟩.
[2] S. Chu, A. Majumdar, Opportunities and challenges for a sustainable energy future, Nature 488 (2012) 294–303, https://doi.org/10.1038/nature11475.
[3] T. Letcher, Comprehensive Renewable Energy, Elsevier, 2022 (https://philpapers.org/rec/LETCRE).
[4] A.G. Olabi, Q. Abbas, A. Al Makky, M.A. Abdelkareem, Supercapacitors as next generation energy storage devices: properties and applications, Energy 248 (2022) 123617, https://doi.org/10.1016/j.energy.2022.123617.
[5] F.-R. Fan, Z.-Q. Tian, Z.L.J.Ne Wang, Flexible Triboelectric Generator 1 (2012) 328–334, https://doi.org/org/10.1016/j.nanoen.2012.01.004.
[6] L. Zhou, D. Liu, J. Wang, Z.L. Wang, Triboelectric nanogenerators: fundamental physics and potential applications, Friction 8 (2020) 481–506, https://doi.org/10.1007/s40544-020-0390-3.
[7] Y. Song, N. Wang, Y. Wang, R. Zhang, H. Olin, Y. Yang, Direct current triboelectric nanogenerators, Adv. Energy Mater. 10 (2020) 2002756, https://doi.org/10.1002/aenm.202002756.
[8] R. Yang, M. Benner, Z. Guo, C. Zhou, J. Liu, High-performance flexible Schottky DC generator via metal/conducting polymer sliding contacts, Adv. Funct. Mater. 31 (2021) 2103132, https://doi.org/10.1002/adfm.202103132.
[9] Z. Zhang, Z. Wang, Y. Chen, Y. Feng, S. Dong, H. Zhou, Z.L. Wang, C. Zhang, Semiconductor contact-electrification dominated tribovoltaic effect for ultrahigh power generation, Adv. Mater. 34 (2022) 2200146 https://doi.org/org/10.1002/adma.202200146.
[10] Y. Lu, Z. Hao, S. Feng, R. Shen, Y. Yan, S. Lin, Direct-current generator based on dynamic pn junctions with the designed voltage output, iScience 22 (2019) 58–69, https://doi.org/10.1016/j.isci.2019.11.004.
[11] C. Xu, J. Yu, Z. Huo, Y. Wang, Q. Sun, Z.L. Wang, Pursuing the tribovoltaic effect for direct-current triboelectric nanogenerators, Energ. Environ. Sci. 16 (2023) 983–1006, https://doi.org/10.1039/d2ee04019k.
[12] J. Liu, A. Goswami, K. Jiang, F. Khan, S. Kim, R. McGee, Z. Li, Z. Hu, J. Lee, T. Thundat, Direct-current triboelectricity generation by a sliding Schottky nanocontact on MoS2 multilayers, Nat. Nanotechnol. 13 (2018) 112–116, https://doi.org/10.1038/s41565-017-0019-5.
[13] Z.L. Wang, A.C. Wang, On the origin of contact-electrification, Mater. Today 30 (2019) 34–51, https://doi.org/10.1016/j.mattod.2019.05.016.
[14] A. Šutka, K. Ma¯lnieks, Mr Zubkins, Ar Plu¯dons, A. Šarakovskis, O. Verners, R. Egli¯tis, P.C. Sherrell, Tribovoltaic performance of TiO2 thin films: crystallinity, contact metal, and thermoelectric effects, ACS Appl. Mater. Interfaces 15 (2023) 33140–33147, https://doi.org/10.1021/acsami.3c05830.
[15] L. Ren, A. Yu, W. Wang, D. Guo, M. Jia, P. Guo, Y. Zhang, Z.L. Wang, J. Zhai, p-n Junction based direct-current triboelectric nanogenerator by conjunction of tribovoltaic effect and photovoltaic effect, Nano Lett. 21 (2021) 10099–10106, https://doi.org/10.1021/acs.nanolett.1c03922.
[16] S. Qin, J. Chen, P. Yang, Z. Liu, X. Tao, X. Dong, J. Hu, X. Chu, Z.L. Wang, X. Chen, A Piezo-tribovoltaic nanogenerator with ultrahigh output power density and dynamic sensory functions, Adv. Energy Mater. 14 (2023) 2303080, https://doi.org/10.1002/aenm.202303080.
[17] W. Qiao, Z. Zhao, L. Zhou, D. Liu, S. Li, P. Yang, X. Li, J. Liu, J. Wang, Z.L. Wang, Simultaneously enhancing direct-current density and lifetime of tribovotaic nanogenerator via interface lubrication, Adv. Funct. Mater. 32 (2022) 2208544, https://doi.org/10.1002/adfm.202208544.
[18] Z. Zhao, J. Zhang, W. Qiao, L. Zhou, Z. Guo, X. Li, Z.L. Wang, J. Wang, Contact efficiency optimization for tribovoltaic nanogenerators, Mater. Horiz. 10 (2023) 5962–5968, https://doi.org/10.1039/d3mh01369c.
[19] J. Meng, Z.H. Guo, C. Pan, L. Wang, C. Chang, L. Li, X. Pu, Z.L. Wang, Flexible textile direct-current generator based on the tribovoltaic effect at dynamic metal-semiconducting polymer interfaces, ACS Energy Lett. 6 (2021) 2442–2450, https://doi.org/10.1021/acsenergylett.1c00288.
[20] L. Zhang, H. Cai, L. Xu, L. Ji, D. Wang, Y. Zheng, Y. Feng, X. Sui, Y. Guo, W. Guo, F. Zhou, W. Liu, Z.L. Wang, Macro-superlubric triboelectric nanogenerator based on tribovoltaic effect, Matter 5 (2022) 1532–1546, https://doi.org/10.1016/j.matt.2022.02.021.
[21] Z. Zhang, L. Gong, R. Luan, Y. Feng, J. Cao, C. Zhang, Tribovoltaic effect: origin, interface, characteristic, mechanism & application, Adv. Sci. 202305460 (2024), https://doi.org/10.1002/advs.202305460.
[22] X. Pan, H. Xiang, Z. Xuan, Y. Jie, X. Cao, Tribovoltaic effect promotes highly efficient direct current generator, J. Mater. Chem. A 11 (2023) 25377–25385, https://doi.org/10.1039/d3ta04807a.
[23] S. Lin, Z. Lin Wang, The tribovoltaic effect, Mater. Today 62 (2023) 111–128, https://doi.org/10.1016/j.mattod.2022.11.005.
[24] M. Zheng, S. Lin, Z. Tang, Y. Feng, Z.L. Wang, Photovoltaic effect and tribovoltaic effect at liquid-semiconductor interface, Nano Energy 83 (2021) 105810, https://doi.org/10.1016/j.nanoen.2021.105810.
[25] Z. Zhang, D. Jiang, J. Zhao, G. Liu, T. Bu, C. Zhang, Z.L. Wang, Tribovoltaic effect on metal–semiconductor interface for direct-current low-impedance triboelectric nanogenerators, Adv. Energy Mater. 10 (2020) 1903713, https://doi.org/10.1002/aenm.201903713.
[26] Y. Lu, Q. Gao, X. Yu, H. Zheng, R. Shen, Z. Hao, Y. Yan, P. Zhang, Y. Wen, G. Yang, S. Lin, Interfacial built-in electric field-driven direct current generator based on dynamic silicon homojunction, Research 2020 (2020) 5714754, https://doi.org/10.34133/2020/5714754.
[27] R. Yang, R. Xu, W. Dou, M. Benner, Q. Zhang, J. Liu, Semiconductor-based dynamic heterojunctions as an emerging strategy for high direct-current mechanical energy harvesting, Nano Energy 83 (2021) 105849, https://doi.org/10.1016/j.nanoen.2021.105849.
[28] M. Zheng, S. Lin, L. Xu, L. Zhu, Z.L. Wang, Scanning probing of the tribovoltaic effect at the sliding interface of two semiconductors, Adv. Mater. 32 (2020) e2000928, https://doi.org/10.1002/adma.202000928.
[29] Y. Liu, Y. Ding, L. Xu, I.W. Jeong, L. Yang, One-step femtosecond laser-induced monocrystalline silicon structure towards enhanced nano-hardness, Mater. Lett. 325 (2022) 132792, https://doi.org/10.1016/j.matlet.2022.132792.
[30] Z. Du, C. Zhang, F. Li, R. Zhou, M. Hong, Impact oF Laser-induced Oxidation on Silicon Wafer Solar Cells' Performance, IEEE J. Photovolt. 6 (2016) 617–623, https://doi.org/10.1109/jphotov.2016.2535243.
[31] T. Menold, E. Hadjixenophontos, R. Lawitzki, G. Schmitz, M. Ametowobla, Crystal defects in monocrystalline silicon induced by spot laser melting, J. Appl. Phys. 127 (2020) 093102, https://doi.org/10.1063/1.5142676.
[32] P. Tománek, P. Škarvada, R. Macků, L. Grmela, Detection and localization of defects in monocrystalline silicon solar cell, Adv. Opt. Technol. 2010 (2010) 1–5, https://doi.org/10.1155/2010/805325.
[33] S. Ferrie, N. Darwish, J.J. Gooding, S. Ciampi, Harnessing silicon facet-dependent conductivity to enhance the direct-current produced by a sliding Schottky diode triboelectric nanogenerator, Nano Energy 78 (2020) 105210, https://doi.org/10.1016/j.nanoen.2020.105210.

Xiongxin Luo received his master degree in Guangxi University. Currently, he is a Ph.D Candidate in Beijing Institute of Nanoenergy and Nanosystems, Chinese Academic of Sciences. His current research interests focus on fabrication and application of ultra-wide band gap semiconductors.

Haixin Li is a Master Degree Candidate in Beijing institute of nanoenergy and nanosystems, school of nanoscience and engineering. University of Chinese Academy of Sciences. Her main research interests are fabrication and application of the nanogenerators.

Andy Berbille is a Ph.D. candidate in Zhong Lin Wang's group at the Beijing Insitute of Nanoenergy and Nanosystems. After graduating from a joint master's program, in Materials Science and engineering, from UPEC, UPEM and ENPC in Paris, France, he was granted a CAS-TWAS President's Fellowship to pursue a Ph.D. degree in the Chinese Academy of Sciences. His research interests cover energy materials, hydrogen storage, heterogeneous catalysis, soft materials, piezoelectric materials, magnetoelectric catalysis and contact-electrification.

Lindong Liu is a Ph.D. Candidate in the School of Civil and Resources Engineering, University of Science and Technology Beijing. His main research interests focus on the fabrication and application of triboelectric nanogenerators.

Yikui Gao received his B. S. degree in Theoretical physics from Chongqing University. Currently, he is a Ph.D. candidate in Beijing Institute of Nanoenergy and Nanosystems, Chinese Academy of Sciences, China. His current research interest is triboelectric nanogenerator.

Gaosi Han is a Ph.D. in Candidate in Beijing Institute of Nanoenergy and Nanosystems, Chinese Academic of Sciences. His main research interests focus on piezoelectric electronics and piezoelectric optoelectronics in perovskites.

Zhong Lin Wang received his Ph.D. from Arizona State University in physics. He is the Hightower Chair in Materials Science and Engineering, Regents' Professor at Georgia Tech. Dr. Wang has made original and innovative contributions to the synthesis, discovery, characterization and understanding of fundamental physical properties of oxide nanobelts and nanowires, as well as applications of nanowires in energy sciences, electronics, optoelectronics and biological science. His discovery and breakthroughs in developing nanogenerators established the principle and technological road map for harvesting mechanical energy from environment and biological systems for powering personal electronics. His research on selfpowered nanosystems has inspired the worldwide effort in academia and industry for studying energy for micro-nanosystems, which is now a distinct disciplinary in energy research and future sensor networks. He coined and pioneered the field of piezotronics and piezo-phototronics by introducing piezoelectric potential gated charge transport process in fabricating new electronic and optoelectronic devices. Details can be found at: http://www.nanoscience.gatech.edu.

Laipan Zhu received his B.S. degree in Physics department from Shandong university in 2010 and his Ph.D. in Institute of Semiconductors, Chinese Academic of Sciences in 2015. He was appointed as an associate professor and a junior professor in Beijing Institute of nanoenergy and nanosystems, Chinese Academic of Sciences, from 2018 and 2023, respectively. His current research mainly focuses on optoelectronics, piezotronics, and nanogenerators.